Articles

Dopant−Host Oxide Interaction and Proton Mobility in Gd:$BaCeO_3$

Francesco Giannici,*,† Alessandro Longo,‡ Antonella Balerna,§ and Antonino Martorana†,‡

Dipartimento di Chimica Inorganica e Analitica "Stanislao Cannizzaro", Università di Palermo, Viale delle Scienze, I-90128 Palermo, Italy, Istituto per lo Studio dei Materiali Nanostrutturati, Consiglio Nazionale delle Ricerche, Via Ugo La Malfa, 153, I-90146 Palermo, Italy, and Laboratori Nazionali di Frascati, Istituto Nazionale di Fisica Nucleare, Via Enrico Fermi 44, I-00044, Frascati, Italy

Received November 3, 2008. Revised Manuscript Received December 24, 2008

The local structure of Gd:$BaCeO_3$ at different dopant concentrations (2−20%) was studied by X-ray absorption spectroscopy. The EXAFS analysis shows that the environment of the regular Ba^{2+} and Ce^{4+} cations is to a limited extent affected by doping. The local structure of gadolinium shows an expansion of the first coordination shell of oxygens, consistent with the ionic radius of Gd^{3+}, but a contraction of the next neighboring shells of cations. In particular, the Ba^{2+} second neighbors get closer to the dopant, which can be originated by the effective negative charge sharply localized on the dopant. Comparison between EXAFS data of dry and hydrated compounds confirms this interpretation, showing a strong interaction of Gd^{3+} with positively charged defects. The environment of gadolinium is compared with the previously investigated local structure of dopants in Y:$BaCeO_3$ and In:$BaCeO_3$. It is observed that yttrium and gadolinium, which induce higher proton conductivity, are characterized by low solubility and strong interaction with positive defects; on the contrary, the lower proton conductivity of In:$BaCeO_3$ coexists with full dopant solubility and insignificant interaction with oxygen vacancies and hydroxyls. A comprehensive interpretation of this behavior is proposed, in terms of a different dopant−host oxide interaction.

1. Introduction

Since the discovery of the high proton conductivity of barium cerate-based compounds by Iwahara and co-workers,[1] the efforts of several research groups have been focused on the improvement of chemical stability and proton diffusivity with the main objective of fabricating solid electrolytes for mature fuel cell technology. In this context, different barium cerate dopants and/or combination of dopants were tried, providing a huge amount of data concerning various features related with conductivity, such as synthesis techniques, processing of materials, microstructure and thermodynamic; these studies concerned in particular yttrium-doped barium cerate, which constitutes the reference compound for high-temperature proton conductors and, despite the poor chemical stability prejudicially affecting technological exploitation, continues to be investigated to obtain deeper insight into the mechanism of solid state proton conduction. Other dopants like gadolinium, in spite of very good conductivity, are much less studied.

$BaCeO_3$ belongs to the wide category of perovskite-like ABO_3 compounds. In the perovskites relevant for solid-state proton conduction, the B cations have charge +4 and coordinate oxygen octahedra, whereas the A^{2+} cations are placed in the cavities formed by the network of corner-sharing octahedra. Protons are introduced in the barium cerate structure by doping the Ce^{4+} site with trivalent M species

$$2Ce_{Ce}^{x} + O_{O}^{x} + M_2O_3 \rightarrow 2M'_{Ce} + V_{O}^{\bullet\bullet} + 2CeO_2 \qquad (1)$$

and dissociative water absorption

$$H_2O + V_{O}^{\bullet\bullet} + O_{O}^{x} \rightarrow 2OH_{O}^{\bullet} \qquad (2)$$

The local structure around a doped B site can be affected by microstrains originated by size mismatch between dopant and substituted cation, but can also be influenced by the interaction of the negatively charged M'_{Ce} defect with first-shell oxygens and with positive charges like B-site cations, oxygen vacancies, or hydroxyls.

In our previous papers, we undertook an accurate investigation of the local structure of barium cerate-based compounds, aiming at understanding possible relations with conductivity.[2−4] The study of yttrium,[2,3] whose hexacoordinated ionic radius (0.90 Å) is almost equal to the one of

* Corresponding author. E-mail: giannici@pa.ismn.cnr.it.
† Università di Palermo.
‡ Istituto per lo Studio dei Materiali Nanostrutturati, Consiglio Nazionale delle Ricerche.
§ Istituto Nazionale di Fisica Nucleare.

(1) Iwahara, H.; Uchida, H.; Ono, K.; Ogaki, K. *J. Electrochem. Soc.* **1988**, *135*, 529.
(2) Longo, A.; Giannici, F.; Balerna, A.; Ingrao, C.; Deganello, F.; Martorana, A. *Chem. Mater.* **2006**, *18*, 5782.
(3) Giannici, F.; Longo, A.; Balerna, A.; Arico, A. S.; Martorana, A. *Solid State Ionics* **2007**, *178*, 587.
(4) Giannici, F.; Longo, A.; Balerna, A.; Kreuer, K.-D.; Martorana, A. *Chem. Mater.* **2007**, *19*, 5714.

10.1021/cm8029888 CCC: $40.75
Published on Web 01/22/2009

cerium (0.87 Å), was followed by the analysis of the local structure of indium, having a much smaller ionic radius (0.80 Å).[4] The comparison of these two barium cerate dopants is quite interesting, as they are antithetical in several aspects involving both structure and properties:

(i) Despite size matching, yttrium can be inserted in the barium cerate matrix to an extent less than 20% of the available B-sites; on the contrary, indium is soluble in any ratio, nevertheless keeping the perovskite-like structure of the host matrix.

(ii) The oxygen octahedral cage around indium is highly regular and the correlation distance of oxygens is definitely contracted with respect to the undoped cerium site (∼2.16 Å vs 2.25 Å, as determined by EXAFS), whereas yttrium presents two different distances from surrounding oxygens (with two neighbors at 2.31 Å and four at 2.23 Å), which could be interpreted as an axial elongation of the YO_6 octahedron.

(iii) The Ba second coordination shell is characterized by a single distance with low structural disorder in In:$BaCeO_3$, whereas the second neighbors of yttrium are spread over a distribution of distances, giving rise to a definitely larger Debye−Waller factor.

(iv) At liquid nitrogen temperature, protons in hydrated Y:$BaCeO_3$ are trapped in the vicinity of yttrium, whereas they are evenly distributed in indium-doped barium cerate.

(v) As is well-known, the highest proton conductivities are achieved by yttrium doping; proton diffusivity in In:$BaCeO_3$ is markedly lower and progressively decreases with the amount of dopant.

It seems unlikely that the limited solubility of yttrium in $BaCeO_3$ can be ascribed only to the aforementioned partial distortion of Y−O distances, whereas it was argued that the much higher solubility of In^{3+} is promoted by easier polarizability, allowing a smooth and progressive release of the strain originated by size mismatch with Ce^{4+}.[4] On the other hand, this electronic flexibility can be detrimental for proton conductivity, likely modifying the lattice dynamics and/or the O−H interaction in the whole oxide network.[5−7] According to this interpretation, the low-temperature proton trapping around yttrium can be a clue about a sharply localized perturbation induced in the host barium cerate matrix by yttrium and involving a strong proton-dopant interaction.[8−10] Thus, the dopant ionic radius seems to be only a minor factor ruling the dopant interaction with barium cerate, whereas the overall electronic structure of the doped oxide could be the key factor controlling proton conductivity;[11] an aspect of the electronic rearrangement induced by dopant insertion in proton conducting perovskites was considered by Kreuer, who proposed that the homogeneous basicity of oxygens in the doped oxide is favorable for proton diffusivity.[12]

With the aim of obtaining further evidence about this analysis, gadolinium-doped barium cerate is investigated by X-ray diffraction to assess sample homogeneity and long-range average structure, and by X-ray absorption spectroscopy to study the local structure around the A and B sites.

Gadolinium is considered a good dopant of barium cerate, yielding proton conductivities similar to yttrium. Despite the experimental problems due to the high neutron absorption cross-section of the Gd nuclei, the structure of Gd:$BaCeO_3$ was investigated by neutron diffraction by Knight and co-workers, who refined the structure of this oxide in the same space group, *Pmcn*, as Y:$BaCeO_3$ and determined that despite the quite large Gd ionic radius (0.94 Å), the average cell is only slightly expanded with respect to the undoped oxide.[13] The conductivity of monocrystalline Gd-doped and Y-doped barium cerate was studied by Kreuer and co-workers, determining that proton diffusivity is similar in the two oxides;[14] Haile and co-workers investigated the conductivity of Gd:$BaCeO_3$ as a fuction of temperature and Ba stoichiometry and proposed that proton−dopant association occurs at low temperatures.[15] The insertion of Gd in barium cerate was investigated by Glöckner and co-workers using computational techniques; in particular, these authors determined a low Gd solution energy in barium cerate and also calculated a strong dopant-vacancy interaction in the dry compound.[16] In more recent years, the research was mainly concerned with the performances[17] and the fabrication techniques[18] of Gd:$BaCeO_3$-based electrolytes.

In this paper, we present the first detailed investigation of the local structure of gadolinium-doped barium cerate demonstrating its consistency with the long-range average structure determined by neutron diffraction[9] and checked on our samples by X-ray diffraction. As a conclusion of our studies mainly focused on the local structure of barium cerate-based protonic conductors, a possible correlation between the interaction of dopant with the host oxide matrix and proton conductivity is also proposed.

2. Experimental Section

2.1. Materials and Synthesis. Barium carbonate (99%, Merck), cerium oxide (99.9%, Alfa Aesar), and gadolinium oxide (99.9%, Alfa Aesar) were used as starting compounds. The powders were mixed in ethanol and calcined at 1100 °C for 2 h, ball milled for 1 h, calcined at 1300 °C overnight, and then planetary milled for 2 h. A portion of the powders was dried in pure N_2 at 700 °C for

(5) Kreuer, K.-D.; Münch, W.; Ise, M.; He, T.; Fuchs, A.; Traub, U.; Maier, J. *Ber. Bunsen-Ges. Phys. Chem.* **1997**, *101*, 1344.
(6) Kreuer, K.-D.; Adams, S.; Münch, W.; Fuchs, A.; Klock, U.; Maier, J. *Solid State Ionics* **2001**, *145*, 295.
(7) Kreuer, K.-D. *Annu. Rev. Mater. Res.* **2003**, *33*, 333.
(8) Islam, M. S.; Davies, R. A.; Gale, J. D. *Chem. Mater.* **2001**, *13*, 2049.
(9) Björketun, M. E.; Sundell, P. G.; Wahnström, G.; Engberg, D. *Solid State Ionics* **2005**, *176*, 3035.
(10) Cordero, F.; Craciun, F.; Deganello, F.; La Parola, V.; Roncari, E.; Sanson, A. *Phys. Rev. B* **2008**, *78*, 054108.
(11) Kreuer, K.-D.; Paddison, S. J.; Spohr, E.; Schuster, M. *Chem. Rev.* **2004**, *104*, 46.
(12) Kreuer, K.-D. *Solid State Ionics* **1999**, *125*, 285.
(13) Knight, K. S.; Bonanos, N. *J. Mater. Chem.* **1994**, *4*, 899.
(14) Kreuer, K.-D; Dippel, T.; Baikov, T. M.; Maier, J. *Solid State Ionics* **1996**, *86−88*, 613.
(15) Shima, D.; Haile, S. M. *Solid State Ionics* **1997**, *97*, 443.
(16) Glöckner, R.; Islam, M. S.; Norby, T. *Solid State Ionics* **1999**, *122*, 145.
(17) Kikuchi, J.; Koga, S.; Kishi, K.; Saito, M.; Kuwano, J. *Solid State Ionics* **2008**, *179*, 1413.
(18) Serra, J. M.; Büchler, O.; Meulenberg, W. A.; Buchkremer, H. P. *J. Electrochem. Soc.* **2007**, *154*, B334.
(19) Larson, A.; Von Dreele, R. B. *General Structural Analysis System (GSAS)*; Los Alamos National Laboratory Report LAUR 86-748; Los Alamos National Laboratory: Los Alamos, NM, 1988.

6 h to completely remove protons, yielding samples labeled as DRY. Another portion was equilibrated in wet N_2 at 300 °C overnight to achieve maximum proton content.

2.2. X-Ray Diffraction. The X-ray diffraction patterns were recorded with a D5005 diffractometer (Bruker) equipped with a graphite monochromator, using Cu Kα radiation in Bragg−Brentano geometry from 18 to 90° 2θ. The diffraction profiles were modeled with GSAS,[19] as previously described for the case of Y:BaCeO$_3$, using an orthorhombic *Pmcn* unit cell.[13] The Gaussian broadening parameters accounting for the instrumental contribution were determined using the LaB_6 standard and fixed during the fit.

2.3. X-Ray Absorption Measurements and Data Analysis. X-ray absorption spectra of hydrated and dry samples from BCG2 to BCG20 were taken in transmission mode at the European Synchrotron Radiation Facility (ESRF): Gd K-edge (50 keV) spectra were collected at BM29 beamline using a Si (311) double-crystal monochromator, whereas Ba and Ce K-edges were taken at GILDA BM8 beamline, using Si(511) crystals. Measurements were taken at 25, 80, and 873 K; at 873 K, the spectra were collected using an in situ thermochemical cell with controlled gas flux.[20]

Standard $BaCeO_3$, Gd_2O_3, and CeO_2 were modeled to obtain reliable S_0^2 and ΔE_0 values. All coordination numbers for cations were fixed, because Schottky defectivity is low. The Ce−M, Gd−M, and Ba−M scattering paths were weighed so to account for random Ce/Gd mixing on the B-site. For Ba and Ce K-edges, the data were weighed by k^2, extracted with a Bayesian algorithm, and fitted with the program Viper,[21] using the theoretical amplitudes and phases calculated by FEFF8.2.[22] In the Ce environment, the model includes four single scattering paths: 6-fold intraoctahedral Ce−O, 8-fold second shell Ce−Ba, 6-fold neighboring octahedra Ce−M1, and 12-fold next-neighboring octahedra Ce−M2. Moreover, the 12-fold multiple scattering path Ce−O−M1 involving corner-sharing octahedra was taken into account. The second Ce−Ba shell is split in two contributions (one 2-fold and one 6-fold) as previously reported for the local structure analysis of similar compounds.[2−4] At 873 K the anharmonic effects on the vibrational behavior of the Ce−O bond must be taken into account. For this reason, the third cumulant was added as a further fitting parameter to allow for the asymmetry of the pair distribution function. In the Ba environment, there are 12 O nearest-neighbors (grouped in three Ba−O average distances), 8 B-sites in the second shell (grouped in two contributions sharing the same disorder factor), and 6 Ba third neighbors (grouped in two as above).

Gd K-edges were modeled using GNXAS, which is particularly suitable for the analysis of disordered systems and then, in this specific case, for the analysis of doingpant environment. A detailed description of this approach, which involves efficient modeling of multiple-scattering paths and bond angles and allows us to take into account multielectron excitations, is given in our previous paper.[2] The fitting model included one Gd−O distance, two Gd−Ba distances, and two three-body Gd−O−M1 contributions with a variable Gd−Ô−M1 angle. The multielectron excitation included in the atomic background was essential to obtain accurate structural results.

3. Results and Discussion

3.1. Gd:BaCeO$_3$ Conductivity. Gadolinium is considered one of the best dopants of barium cerate, giving conductivities similar to those measured for Y:BaCeO$_3$ or even better, depending on the electrolyte processing. The conductivity of $BaCe_{0.9}Gd_{0.1}O_{3-x}$ in wet N_2 atmosphere at 300 °C is about 1 mS/cm. In the same experimental conditions, the conductivities of $BaCe_{0.9}Y_{0.1}O_{3-x}$ and $BaCe_{0.9}In_{0.1}O_{3-x}$ are about 1 and 0.2 mS/cm, respectively.

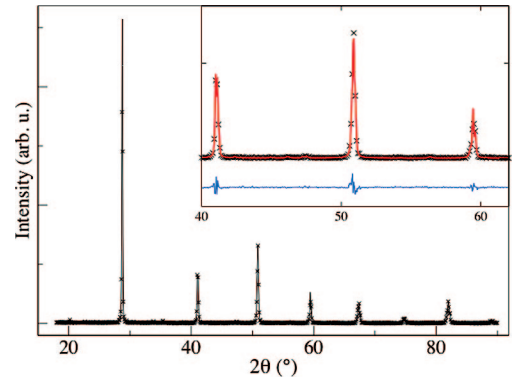

Figure 1. X-ray diffraction pattern of BCG10. In the insert, a detail of the fitting.

3.2. Long-Range Order in Gd:BaCeO$_3$. The average structure of Gd:BaCeO$_3$ was attributed by Knight and coworkers to the *Pmcn* space group.[13] In Figure 1 the experimental X-ray powder pattern of the 10% Gd-doped sample is reported; no secondary phases or amorphous components are observed. As can also be appreciated in the inset of Figure 1, the fitting in the *Pmcn* space group is thoroughly satisfactory and gives cell parameters in agreement with the literature; in particular, the equivalent cubic cell parameter is nearly constant as a function of the Gd content.[13,15] It is worth noticing that the corresponding parameter of In:BaCeO$_3$ definitely decreases with increasing dopant concentration.[4]

3.3. Local Environment of Undoped Cationic Sites. Table 1 reports the analysis relative to the EXAFS spectra of samples BCG2, BCG10 and BCG20 taken at 25 K. At 80 K the results are essentially similar, but for higher Debye−Waller factors. The EXAFS spectrum and the calculated oscillations relative to the sample BCG10 are drawn in Figure 2. In particular, it is evident the high quality of the data taken at 25 K, allowing to obtain a very high degree of structural resolution. From inspection of Figure 3, reporting the Fourier transforms (FT) of the EXAFS signals of Figure 2, it is clear that the model of local structure about cerium contains signals on a wide frequency range. The residual in Figure 2 is originated from a high frequency components at 7 Å and beyond, as is shown in the model FT drawn in Figure 3. On the basis of the Ce K-edge results, it can be observed that the CeO_6 octahedra are characterized by a single Ce−O distance, not affected by Gd concentration; the contraction of the Ce-M1 distance, recognizable in the samples with the higher dopant content, should be ascribed to the smaller Ce−O−M1 angle when M1 = Gd (vide infra, the analysis of Gd environment). Regarding the Ce−O−M1 configuration, its length, reported in the ninth column of Table 1, is geometrically determined by the average tilting angle: the latter being lower than 180°, the Ce−O−M1 path is always slightly longer than the direct Ce−M1 distance. This indirectly confirms the local orthorhombic distortion.

(20) Longo, A.; Balerna, A.; D'Acapito, F.; D'Anca, F.; Giannici, F.; Liotta, L. F.; Pantaleo, G.; Martorana, A. *J. Synchrotron Radiat.* **2005**, *12*, 499–505.
(21) Klementev, K. D. *J. Phys. D: Appl. Phys.* **2001**, *34*, 209.
(22) Ankudinov, A. L.; Ravel, B.; Rehr, J. J.; Conradson, S. D. *Phys. Rev. B* **1998**, *58*, 7565.

Table 1. Structural Parameters of Ce^{4+} Local Environment in BCG at 25K Derived from EXAFS Analysis; Distances in Å, Debye-Waller factors in 1×10^{-3} Å^2; Uncertainty is on the Last Digit

	Ce−O		Ce−Ba ($N = 2$)		Ce−Ba ($N = 6$)		Ce−M1		Ce−O−M1	Ce−M2	
	R	σ^2	R	σ^2	R	σ^2	R	σ^2	R	R	σ^2
BC	2.25	3.0	3.71	3.0	3.85	6.1	4.43	2.2	4.48	6.23	2.0
BCG2	2.25	4.5	3.70	4.4	3.84	7.9	4.43	3.3	4.47	6.22	2.3
BCG2DRY	2.25	4.3	3.70	4.1	3.84	7.6	4.42	3	4.46	6.22	2
BCG10	2.24	4.5	3.73	3.9	3.87	6.9	4.28	3	4.37	6.22	2.7
BCG10DRY	2.25	5.0	3.70	4.4	3.85	7.1	4.27	2.6	4.36	6.23	2.4
BCG20	2.24	4.7	3.71	4.3	3.86	7.2	4.28	3.6	4.37	6.25	3
BCG20DRY	2.25	4.4	3.69	5.5	3.83	7.7	4.27	3.3	4.37	6.23	2.8

Table 2. Structural Parameters of Ba^{2+} Local Environment in BCG at 25K Derived from EXAFS Analysis; Distances in Å, Debye−Waller Factors in 1×10^{-3} Å^2; Uncertainty is on the Last Digit

	Ba−O ($N = 4$) Ba−O ($N = 5$)			Ba−O ($N = 3$)		Ba−M	Ba−M Ba−Ba			Ba−Ba	
	R	σ^2	R	R	σ^2	R	R	σ^2	R	R	σ^2
BC	2.72	28	2.85	3.61	9.2	3.73	3.86	5.1	4.40	4.46	6.2
BCG2	2.77	22	2.85	3.62	16	3.73	3.86	5.7	4.37	4.45	7.9
BCG2DRY	2.75	26	2.83	3.64	13	3.73	3.87	5.8	4.36	4.48	7.8
BCG10	2.78	27	2.87	3.64	14	3.73	3.85	6.0	4.35	4.47	8.2
BCG10DRY	2.76	24	2.87	3.65	14	3.74	3.87	5.8	4.35	4.47	8.1

The disorder factor of the Ce−O−M1 was constrained to the Ce−O one. The average fourth-shell Ce−M2 distance remains almost unperturbed with increasing Gd^{3+} content, demonstrating that there is no long-range expansion or contraction of the whole lattice within the EXAFS sensitivity. Figure 4 shows the effect of high temperature on the EXAFS oscillations of BCG10 and in particular that the surviving signal is essentially due to the octahedral oxygens directly bound to Ce^{4+}. At 873 K, the CeO_6 octahedron remains symmetric, with a slightly elongated bond of 2.28 Å and a Debye−Waller factor $\sigma^2 = 0.009(3)$ Å^2. The values of the higher cumulants are $C_3 = 1 \times 10^{-3}$ Å^3 and $C_4 = 3 \cdot 10^{-4}$ Å^4. For comparison, in the same conditions, the Ce−O first shell in BCY10 is a bit shorter (2.26 Å), less disordered ($\sigma^2 = 0.007(2)$ Å^2), and the motion is less anharmonic ($C_3 = 6 \times 10^{-4}$ Å^3).

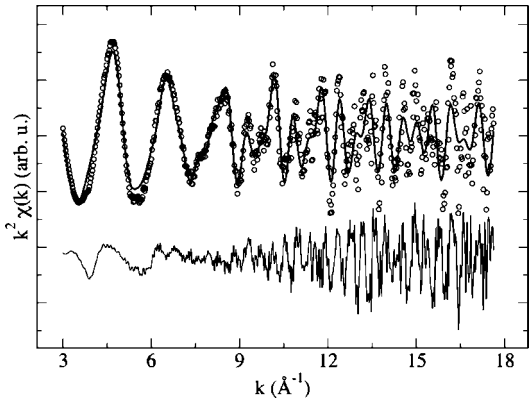

Figure 2. Experimental (open circles) k^2-weighted EXAFS spectrum of BCG10 at the Ce K-edge.

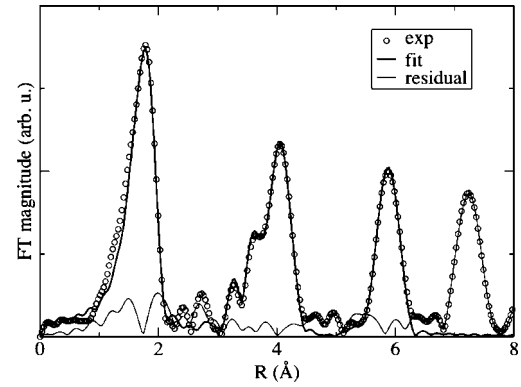

Figure 3. Fourier transforms of the functions drawn in Figure 2.

Also the Ba K-edge data are of very high quality. The substantial independence of the local structure on the dopant content holds also for the A cations, as proved by the results relative to the Ba K-edge shown in Table 2.

3.4. Local Environment of Gd^{3+} Dopant. Figure 5 shows the EXAFS oscillations at the Gd K-edge of BCG10 and in particular the contribution of a multielectron excitation, modeled with a Lorentzian function;[23] the experimental spectrum, cleared of the multiple excitation, and the signal calculated under the assumption of Gd insertion in the B site of $BaCeO_3$, are drawn in Figure 6. The very good fitting demonstrates that within the EXAFS sensitivity, it is unlikely that gadolinium goes into the A site. The EXAFS results on the Gd K-edge are reported in Table 3. Here, the three-body Gd−O−M configurations were refined by fitting the corre-

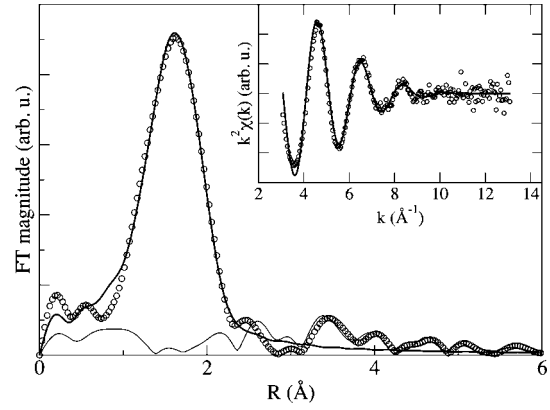

Figure 4. Fourier transform (open circles) of the k^2-weighted EXAFS spectrum of BCG10 at the Ce K-edge; the data are taken at 873 K. In the inset, the corresponding the k^2-weighted EXAFS spectrum and model.

sponding tilting angle and the angle variance, so that the direct Gd−M distances and disorder factors were geometricaly derived without adding further fitting parameters. By inspection of Table 3, the Gd−O bond lengths are longer than the corresponding Ce−O distances, both in undoped barium cerate and in Gd:BaCeO$_3$ (Table 1), as it is expected because hexacoordinated Gd^{3+} is larger than Ce^{4+}.[24] As a consequence, the volume of the oxygen cage around gadolinium increases, depending on the samples, in the range 7−12% with respect to the undoped B-site. It is worth observing that the volume of the oxygen cage of indium in

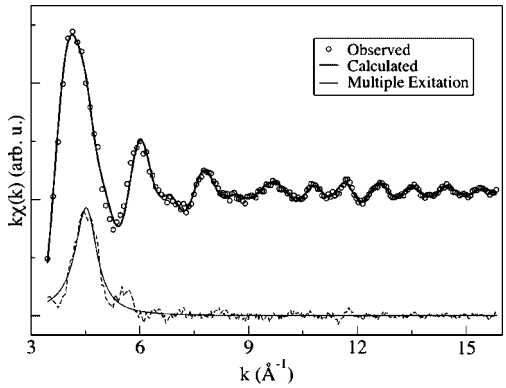

Figure 5. k^2-weighted EXAFS spectrum of BCG10 at the Gd K-edge; the data taken at 25 K. The multielectron excitation, modeled with a Lorentzian profile, is drawn. The dashed line represents the difference between the experimental signal and the overall (calculated + multiple excitation) model.

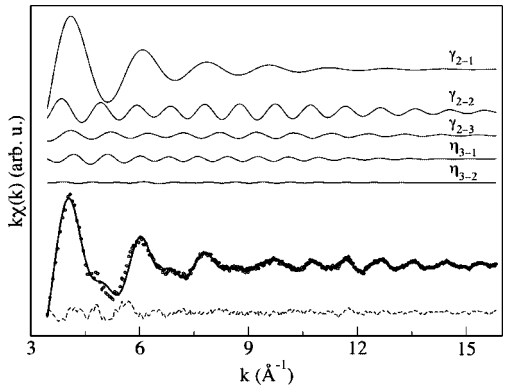

Figure 6. Components of the calculated EXAFS signal (upper panel) and fit to the experimental Gd K-edge EXAFS signal of BCG10 cleared of the multielectron excitation.

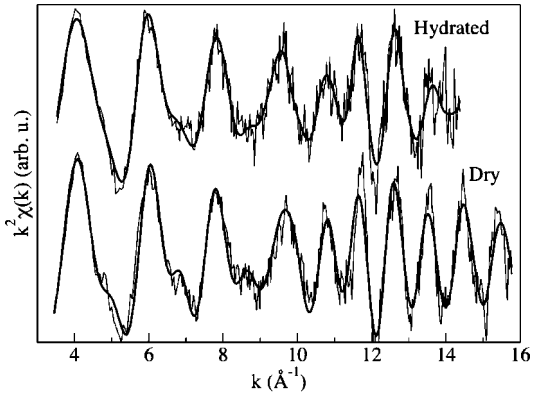

Figure 7. Comparison between the EXAFS signals and the respective fitted models for dry and hydrated BCG10.

In:BaCeO$_6$ is consistent with In^{3+} hindrance, showing a contraction of about 15% with respect to the regular B-site;[4] the farther coordination shells are also contracted, but the difference relative to the undoped B-site progressively decreases, so allowing a smooth release of the strain originated by the small ionic radius of indium.[4] It is then quite surprising that despite the larger hindrance of the GdO$_6$ octahedron, the Gd−Ba and Gd−M shells are closer to gadolinium, in wet and dry BCG samples as well, with respect to the corresponding shells involving indium.

Taking into account the dopant ionic radius, it is clear that the smaller size of indium locally allows a more symmetric arrangement of Ba^{2+} cations, according to the crystallographic analysis of ion packing in perovskites,[25] whereas insertion of gadolinium involves a structural misfit originated by a large discrepancy from the ideal Goldschmidt cation size. This trouble can be recognized in the Gd−O−M angles (Table 3), generally smaller than the corresponding Ce−O−Ce angles in the undoped oxide (∼160°) and clearly originated by a larger tilting of the Gd-centered oxygen octhedra. This modification leave the first shell Ce−O and Gd−O bonds almost unperturbed, so that it is likely that the CeO$_6$ and GdO$_6$ octahedra are somewhat rigid in their tilting. The observed contraction of the cationic shells around Gd could then be (at least, partially) ascribed to a geometrical rearrangement. On the other hand, all the second shell Gd−Ba lengths reported in Table 3 are shorter than the corresponding Ce−Ba distances (Table 1), whereas smaller M−O−M angles, as can be recognized in homologous series of perovskites with increasing Goldschmidt tolerance factor (for instance, the series CaZrO$_3$−SrZrO$_3$−BaZrO$_3$ or SrCeO$_3$−BaCeO$_3$), give rise to a range of longer and smaller B−A correlations, with an average B−A distance increasing with the size of the A cation. It then seems feasible to envisage that the collapse of the Ba^{2+} shell toward Gd^{3+} could also depend on the excess negative charge on the acceptor dopant. A similar effect is also observed in Y:BaCeO$_3$,[2] even if the Y−Ba average distance contraction takes place to a lesser extent ($\langle d_{Y-Ba}\rangle$ = 3.76 Å and $\langle d_{Gd-Ba}\rangle$ = 3.55 Å, vs $\langle d_{Ce-Ba}\rangle$ = 3.82 Å in undoped BaCeO$_3$), probably because the structural rearrangement in this case is very limited because of the nearly equal size of Ce^{4+} and

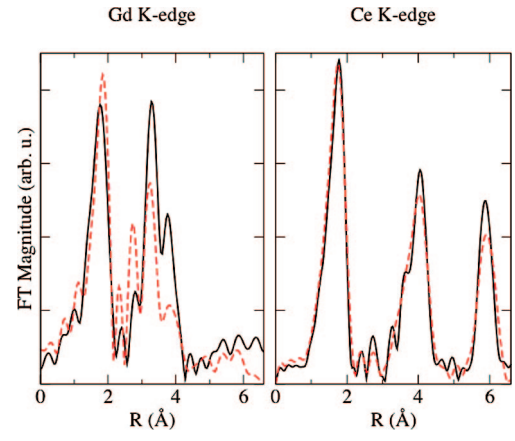

Figure 8. (a) Fourier transforms for dry (black solid line) and hydrated (red dashed line) BCG10 at the Gd K-edge. (b) Hydrated and dry BCG10 at the Ce K-edge.

Table 3. Structural Parameters of Gd^{3+} Local Environment in BCG at 25K Derived from EXAFS Analysis; Distances in Å, Debye-Waller Factors in 1×10^{-3} Å^2; Uncertainty is on the Last Digit

	Gd−O		Gd−Ba ($N = 2$)		Gd−Ba ($N = 6$)	Gd−O−M		Gd−M		Gd−O−M		Gd−M	
	R	σ^2	R	σ^2	R	θ	σ_θ	R	σ^2	θ	σ_θ	R	σ^2
BCG10	2.33	3.9	3.41	6.3	3.59	137	3	4.32	8.4	141	6	4.38	6.7
BCG10DRY	2.30	4.4	3.44	4.0	3.58	136	2	4.26	6.2	143	3	4.37	4.7
BCG20	2.32	4.4	3.44	6.4	3.61	127	1	4.12	8.8	140	11	4.36	
BCG20DRY	2.34	3.8	3.43	4.7	3.61	124	1	4.12	6.1	142	10	4.41	

Y^{3+}. The possible Ba shell collapse in In:$BaCeO_3$ originated by an effective negative charge on the dopant is overcome by the adjustment of the structure to the small indium-centered oxygen cage,[4] and therefore it is not possible to draw conclusions about the electronic charge rearrangement about indium, on the basis of the analysis the In−Ba and In−M distances.

A support to the hypothesis that an effective negative charge resides on gadolinium, can be found by comparison between the EXAFS spectra of dry and protonated 10% Gd-doped $BaCeO_3$ reported in Figure 7; in particular, different positions of the maxima and weaker oscillations at large k-values can be observed for hydrated BCG10. An evident difference in the respective radial functions of BCG10 and BCG10DRY at the Gd site can be easily recognized in the left panel of Figure 8, confirming that the local environment of the doped B-sites is largely perturbed upon hydration/dehydration; at the Ce K-edge, shown in the right panel of Figure 8, no significative change can be recognized. By inspection of Table 3, both bond lengths and disorder factors are affected, the latter being about 20−60% lower in dry samples. It seems plausible that the difference between dry and hydrated BCG10 could be ascribed to a sharply localized negative charge on the dopant, which is able to attract the positively charged defects, i.e., vacancies in dry samples and/or hydroxyls in the hydrated ones. It is worth pointing out that a similar effect was observed also for yttrium doping,[2] whereas no specific structural difference between dry and protonated samples was observed in the vicinity of the dopant for indium-doped barium cerate.[4]

On the basis of the literature on cerates and zirconates,[4,6,11] and of the results reported in this paper, the relevance of ionic radius matching for proton diffusivity in acceptor-doped perovskites can be definitely ruled out; on the other hand, the importance of the electronic structure of the doped oxide has been recognized in computational and experimental approaches. In particular, Kreuer proposed that "chemical matching" of dopant should be more critical for proton mobility than size matching, meaning that a good dopant should not modify the basicity of the host oxide.[6] This hypothesis was also investigated by Islam and co-workers, who found increasing proton binding energies at the B site of $CaZrO_3$ doped, respectively, with Ga^{3+}, In^{3+}, and Sc^{3+}.[8] It can be argued that according to the idea of "chemical matching", high proton mobility is essentially a property of the host oxide, that could be biased by dopant insertion, if a general and appreciable modification of the O−H interaction and of the lattice dynamics are involved.

The local structure analysis of three different dopants of barium cerate substantiate this analysis. Considering the problem from the point of view of dopant insertion, it could be put forth that the requisite for a good dopant is "chemical mismatch", meaning that it should be included in the host network as a sharply localized perturbation, leaving unmodified the general electronic structure of the oxide matrix: then, Y^{3+} and Gd^{3+} are pushed into barium cerate and allow hydration at the cost of low solubility and strong interaction with positive defects. On the contrary, the full solubility and negligible interaction of indium with vacancies and hydroxyls depend on the ability of In^{3+} of mimicking the substituted Ce^{4+} cation through a delocalized rearrangement of the electronic structure of the doped oxide.

4. Conclusions

The long-range structure of Gd-doped barium cerate is only slightly depending on the dopant concentration, as proved by the tiny variation in the cell volume of samples with a nominal Gd amount ranging from 2 to 20% of the available B-sites. To the best of our knowledge, 20% is probably even larger than the maximum Gd solubility and this is indicative of a troublesome insertion in the barium cerate network. According to the experimental evidence reported in this paper, the weak dependence of the average cell constants on the dopant concentration can be explained on the basis of the local structure analysis, taking into account that the increased volume of the GdO_6 octahedra is effectively counterbalanced by a contraction of the farther coordination shells. This strong perturbation around the dopant could be one of the sources of the reduced Gd solubility in barium cerate.

In comparison with indium, gadolinium is a better dopant, bringing about a definitely larger proton mobility. The local structure analysis demonstrates that, at the low temperature of the EXAFS experiment, positive defects inserted in the structure are trapped, like in Y-doped barium cerate, in the vicinity of the dopant. On the contrary, no preferential attraction for protons or oxygen vacancies is exhibited by indium. It is then proposed that the greater chemical homogeneity of the indium-doped oxide depends on a spread of the excess negative charge on the dopant throughout the host lattice that, on the one hand, enhances solubility but that, on the other hand, biases the proton diffusivity by a modification of the proton−oxide interaction delocalized on the whole In:$BaCeO_3$ network.

As a consequence of the present analysis concerning the local structure of Gd-doped barium cerate and the comparison with the behavior of indium and yttrium, one can put forth

(23) Kodre, A.; Arcon, I.; Padeznik Gomilsek, J.; Preseren, R.; Frahm, R. *J. Phys. B* **2002**, *35*, 3497.
(24) Shannon, R. D. *Acta Crystallogr., Sect. A* **1976**, *32*, 751.
(25) Glazer, A. M. *Acta Crystallogr., Sect. A* **1975**, *31*, 756.

that proton diffusivity is essentially a property of barium cerate. Good dopants like yttrium and gadolinium allow us to introduce protons in the oxide structure with minor modification, except for the local environment, of the electronic and/or atomic structure of the host matrix. A worse dopant like indium can be inserted in any ratio in the B-sites of barium cerate at the cost of a substantial modification of the electronic structure of the oxide, affecting O−H interaction and lattice dynamics.

Acknowledgment. We acknowledge the European Synchrotron Radiation Facility for provision of synchrotron radiation and we thank the technical and scientific staff of beamlines BM29 and GILDA BM8. We thank Francesco Giordano (ISMN-CNR) for XRD measurements, and Dr. Klaus-Dieter Kreuer (MPI-FKF, Stuttgart) for useful discussions. Partial financial support from Ministero dell'Università e della Ricerca (PRIN 2006 Ceramici protonici per celle a combustibile and FISR Progetto celle a combustibile) and from Università di Palermo (ex 60%) is acknowledged.

CM8029888